forests

MDPI

Article

Investigations into the Efflorescence of the Treated Wood of the *Iulia Felix* Roman Wreck and Effects of Environmental Conditions on Its State

Elisa Pecoraro [1], Nicola Macchioni [1], Giorgia Musina [2], Emma Cantisani [3], Sveva Longo [4], Marta Novello [5] and Benedetto Pizzo [1,*]

[1] National Research Council of Italy, Institute of Bioeconomy (CNR-IBE), via Madonna del Piano 10, I-50019 Sesto Fiorentino, FI, Italy; elisa.pecoraro@cnr.it (E.P.); nicola.macchioni@cnr.it (N.M.)
[2] Soprintendenza Archeologia, Belle Arti e Paesaggio per il Friuli Venezia Giulia (SABAP-FVG), Piazza Libertà 7, I-34135 Trieste, TS, Italy; giorgia.musina@cultura.gov.it
[3] National Research Council of Italy, Institute of Heritage Science (CNR-ISPC), via Madonna del Piano 10, I-50019 Sesto Fiorentino, FI, Italy; emma.cantisani@cnr.it
[4] National Research Council of Italy, Institute of Heritage Science (CNR-ISPC), via Biblioteca 4, I-95124 Catania, CT, Italy; sveva.longo@cnr.it
[5] Museo Storico e Parco del Castello di Miramare-Direzione Regionale Musei Nazionali Friuli Venezia Giulia (MU MIRA-DRM-FVG), Museo Archeologico Nazionale di Aquileia, via Roma 1, I-33051 Aquileia, UD, Italy; marta.novello@cultura.gov.it
* Correspondence: benedetto.pizzo@cnr.it

Abstract

The *Iulia Felix* is a 2nd-century AD Roman shipwreck that was discovered off the coast of Grado in 1986. Following its recovery, the hull was dismantled and treated with high concentrations of PEG 4000 at elevated temperatures. This process was completed in 2003. The elements were then stored for over 20 years. During this prolonged storage period, salt efflorescence developed on some surfaces, raising concerns about ongoing degradation and prompting an investigation into the composition of the wood and how environmental conditions influence it. The efflorescence was analysed using scanning electron microscopy with energy dispersive spectroscopy (SEM-EDS), X-ray powder diffraction (XRPD) and Fourier transform infrared spectroscopy (FTIR). To evaluate the impact of environmental factors, samples were exposed to controlled humidity levels of 35% and 85% until equilibrium was achieved. The analyses identified iron- and sulphur-based compounds, including hydrated ferrous sulphates, calcium sulphate and hydrated iron oxides. These findings suggest a corrosion-related degradation process that originates in a marine burial environment and progresses in humid, oxygen-rich conditions after recovery. The presence of PEG within the efflorescence indicates that environmental conditions after treatment promoted its gradual migration to the surface. Climate testing revealed that PEG 4000 significantly reduced hygroscopic exchange with the environment. Under dry conditions, dimensional changes were minimal, with less than 1% variation in mass and surface area. In contrast, prolonged exposure to high humidity resulted in a 11% increase in mass due to moisture uptake, as well as a roughly 5% increase in surface area. This was accompanied by minor cracking and, in some cases, structural failure. This study highlights the long-term conservation challenges posed by waterlogged archaeological wood treated with high-molecular-weight PEG. It emphasises the importance of continuous environmental monitoring to mitigate degradation processes and preserve structural integrity, providing valuable insights for future museum conservation strategies.

Check for updates

Academic Editor: Alain Cloutier

Received: 25 April 2026
Revised: 15 May 2026
Accepted: 19 May 2026
Published: 21 May 2026

Copyright: © 2026 by the authors. Licensee MDPI, Basel, Switzerland. This article is an open access article distributed under the terms and conditions of the Creative Commons Attribution (CC BY) license.

Keywords: waterlogged archaeological wood; wood consolidation; PEG 4000; iron and sulphur compounds; moisture exchanges

1. Introduction and Research Aims

The 2nd-century AD Roman wreck of Grado, known as *Iulia Felix*, was discovered in 1986, six miles off the coast of Grado in the province of Gorizia in north-eastern Italy, at a depth of 15 m. Underwater excavations began in 1987 and continued until 1999, culminating in the complete recovery of the hull and its cargo [1–3].

The *Iulia Felix* was a cargo ship mainly carrying sauces and other fish-processing products preserved in amphorae and glassware fragments [4,5] intended for remelting. As excavation progressed and stratigraphic layers were removed, the nearly complete outline of the ship emerged, including its frames, planking (both internal and external courses), as well as well-preserved sections of the keel and keelson. The keelson, a long beam positioned over the frame floors, served to connect and strengthen the longitudinal structure of the ship. Structurally, the wood appeared well-preserved up to the junction with two stern posts and two stem posts.

Following its recovery, the planned consolidation and restoration project originally aimed to treat the wreck as a whole. However, due to logistical and meteorological challenges, these original plans changed, and the hull was disassembled while still submerged [6]. The individual components were initially stored in a tank for desalination and subsequently treated with polyethylene glycol (PEG) with average molecular weight of 4000 g/mol (PEG 4000). Based on the limited documentation available, the treatment commenced with low concentrations (10% in water) at room temperature, gradually increasing to high concentrations and temperatures, which were maintained until the impregnation process was complete. Treatment and drying were finished in 2003. While awaiting exhibition in the Museo nazionale di archeologia subacquea dell'Alto Adriatico (i.e., the National Museum of Underwater Archaeology of the Upper Adriatic), specifically designed in Grado, the wreck elements have remained in storage (Figure 1). The museum opened to the public at the end of 2025, but work on the interior will continue over the coming months [7]. More than 20 years have passed since the conservation of the hull elements. Given the need to establish new exhibition conditions, it is necessary to assess how the treated artefact will interact with the museum's new environment and determine the optimal layout.

Figure 1. Aspect of some of the wooden elements that were stored in the stockroom for over 20 years (**a**) and an example of the efflorescence that appeared on the surface of some of the elements (**b**).

This interaction will affect the exhibition conditions. In fact, the prolonged storage of the wreck over time has introduced new variables that affect its conservation, making this reassessment particularly pertinent. In particular, salt efflorescence has recently appeared on the surfaces of some of the disassembled elements, raising concerns about potential further degradation (Figure 1).

Efflorescence results from the precipitation of salts from a supersaturated state within a porous substrate such as wood, particularly when the liquid–vapour interface remains at the surface. Among the inorganic compounds commonly found in marine archaeological wooden artefacts, iron and sulphur compounds are particularly prevalent [8,9]. These compounds originate from the corrosion of iron nails, or other sources of iron ions, and the action of sulphur-reducing bacteria. They tend to accumulate near the surface, posing a dual threat: mechanical damage and catalytic effects that may trigger oxidative degradation. This degradation process can potentially compromise both the wood structure and the consolidating agents, such as PEG [10]. This ultimately affects the artefact's long-term physicochemical and aesthetic stability, i.e., the absence of chemical alteration, surface changes or adverse interactions with the environment (e.g., efflorescence formation). A recent study on the Yenikapı 12 shipwreck [11], also treated with PEG, highlighted the challenges posed by sulphur and iron accumulation in waterlogged wood (WW), emphasising the need for continuous monitoring and tailored conservation strategies [11]. The research demonstrated how chemical interactions between PEG, sulphur compounds, and iron can contribute to the degradation of archaeological wooden materials over time, reinforcing the necessity for ongoing monitoring and customised conservation approaches. Other scientific studies of salt deposits in WW have been conducted on notable shipwrecks such as the Skuldelev ships and the Vasa, which were treated with PEG [12].

Over the past 50 years, PEG has been the most widely utilised consolidant for WW due to its cost-effectiveness and satisfactory results. However, it has also revealed significant limitations. Chemical interactions with environmental factors—including high humidity levels—can expedite wood degradation [13,14]. PEG reactions with metal and sulphur compounds found in WW can generate low-molecular-weight organic acids (formic, glycolic, and oxalic acids), further contributing to wood degradation [15,16]. Moreover, PEG's hygroscopic nature can result in dimensional variations such as shrinkage and cracking when subjected to fluctuating humidity levels [17–19].

Therefore, assessing the state of preservation of artefacts that have already been treated with PEG, such as the *Iulia Felix*, is a very important issue in the conservation of Cultural Heritage. In this case, a new approach to implementing a suitable diagnostic plan is required to assess the potential advancement of artefact degradation. This subject will be addressed in a separate study [20]. In this case, given the potential modification of PEG in the studied case, which could affect its long-term physicochemical and aesthetic stability, it is important to evaluate the actual response of the treated material to humidity fluctuations. This response potentially differs from that expected for artefacts treated with PEG 4000 due to the mentioned possible changes in its structure.

In addition to wood, the characterisation of salt efflorescence is also an important step in this diagnostic plan. This type of characterisation is well documented in WW. Analytical protocols typically include XRF, EDS, ICP-AES and depth profiling of key ions in the wooden matrix [21–23]. However, these techniques usually only identify the deposited ions, whereas other methods, such as XRD and advanced spectroscopy (including ATR-FTIR and Raman spectroscopy) are more suitable for identifying the molecular structure of salt efflorescence [21–23]. On the other hand, only a few techniques, such as synchrotron-based X-ray absorption spectroscopy (XANES), enable precise speciation of sulphur and iron compounds [24].

The aim of the present work was to identify the chemical nature of the efflorescence that appeared on the surface of certain elements of the *Iulia Felix* wreck during their long-term storage after treatment, in an attempt to understand its origin. Moreover, the study aimed to determine the effects of humidity fluctuations on the dimensional stability of the wooden elements in preparation for their display in the Museum's new environment.

2. Materials and Methods

2.1. Wood Samples

Wooden samples were collected from various parts of the disassembled hull, which is preserved in the National Museum of Underwater Archaeology of the Upper Adriatic deposit in Grado (TS) (Table 1). Given the importance of the artefact, the size of the samples was small and variable. The samples had an equivalent diameter of approximately 10–30 mm (transversal wood section) and a length of approximately 20–60 mm (along the longitudinal wood direction). The hull elements had previously been treated with PEG 4000. Details of the wood species identification are reported in a separate paper [20]. As shown in Table 1, most of the elements were softwoods, predominantly *Pinus pinea* L. (stone pine), which was used for various components, including the secondary keelson, splinter fragments, stem, upper planking, parts of frames (partial frames) and frame floors. *Pinus sylvestris* L. (Scots pine) was also common, having been used for parts of the bow and various planking elements (T8 E, T7 W and T4 W). In contrast, the stern wheel fragment, another bow element and a lateral component (F14 E PP) were made of *Larix decidua* Mill. (larch) [3]. Some elements reflected a more selective use of different species: the belaying pin was made from *Olea europaea* L. (olive wood), and the keel was made from *Ulmus* spp. (elm).

Table 1. List of the collected wood samples and wood identification.

Sample ID	Element Type (Where Available) and Museum Reference Number	Wood Species
6	Secondary keelson—E PE 10/11	*Pinus pinea*
8	Belaying pin	*Olea europaea*
9	Splinter	*Pinus pinea*
11	Bow—T6 E (2)	*Pinus sylvestris*
12	Stem—M34 W ST	*Pinus pinea*
13	Partial frame—M34 E SE	*Pinus pinea*
14	Stern wheel (keelson fragment)	*Larix decidua*/*Picea abies*
15	Upper planking/spare—T6 E	*Pinus pinea*
16	Frame floor—M47 CW M	*Pinus pinea*
17	Partial frame—M47 E SE	*Pinus pinea*
18	Partial frame—M47 W SE	*Pinus pinea*
20	T8 E	*Pinus sylvestris*
21	T7 W	*Pinus sylvestris*
22	Bow—T7 E	*Larix decidua*/*Picea abies*
23	Keel	*Ulmus* spp.
24	F14 E PP	*Larix decidua*/*Picea abies*
25	T4 W	*Pinus sylvestris*

2.2. Characterisation of Surface Efflorescence

A separate set of four samples was collected where mineral efflorescence was more abundant: M12 W ST (stem), M48 E SE (semi-frame), F14 E PP and T6 E (see Table 2). The material was gathered from the surface of each element, as illustrated in the photographs in Table 2. The efflorescence varied in colour from yellowish to white, with reddish/brown concretions.

Table 2. List of hull elements with abundant surface efflorescence that were sampled.

Museum Reference Number	Element Type from Which the Samples Were Taken (Where Available)	Photo
T6 E	Bow	
M48 E SE	Partial frame	
F14 E PP	-	
M12 W ST	Stem	

Three sets of analyses were conducted on the powders: (a) microanalysis using a scanning electron microscope (SEM) equipped with an energy-dispersive spectroscopy (EDS) probe, (b) X-ray powder diffraction (XRPD), (c) Attenuated Total Reflectance Fourier-Transform Infrared Spectroscopy (ATR-FTIR). Before the analyses, the powders were finely ground in an agate mortar, and any coarse particles containing recognisable wood residues were removed.

2.2.1. EDS Analysis

Microanalysis investigated efflorescence using a scanning electron microscope (SEM) equipped with an energy-dispersive spectroscopy (EDS) probe. The SEM analysis employed a TESCAN GAIA3 (TESCAN, Brno, Czech Republic) with a Ga-based Triglav column and focused ion beam (FIB) technology. The microscope featured an EDS probe that enabled elemental identification in the four analysed powder samples. The analyses were carried out under a voltage of 10 kV. The presence of iron and sulphur contamination was specifically examined.

2.2.2. XRPD Analysis

X-ray powder diffraction (XRPD) was carried out using an X'Pert Pro PANalytical diffractometer (Malvern Panalytical, Worcestershire, UK) equipped with an X'Celerator detector with a Cu X-ray tube (λ = 1.54 Å) and with a Ni-filtered Cu–Kα radiation source.

The X-ray tube was operated at 40 kV and 30 mA. The diffraction patterns were collected from 3–70° 2θ with a step size of 0.02° and total time per pattern of 16 min 27 s. A sample stage zero-background was used. For phase identification of XRPD results the Powder Diffraction (PDF) database from the International Center for Diffraction Data (ICDD) was used.

2.2.3. FTIR Analysis

The efflorescence was also analysed by FTIR spectroscopy. FT-IR spectra were acquired using a Fourier transform spectrometer (Bruker Optics, mod. Alpha, Karlsruhe, Germany) equipped with an attenuated total reflectance (ATR) system. The spectral range for acquisition was from 4000 to 400 cm^{-1}, with a resolution of 4 cm^{-1}. A total of 40 successive scans were averaged. Spectra were processed using OPUS 9.1 software (Bruker Optics, 2025).

2.3. Conditioning Tests

To assess the effect of environmental conditions on the treated finds, thin slices (approximately 7 mm thick) were obtained from the collected wood samples (Table 1). The slices were cut only along the longitudinal direction, while the transversal section remained unchanged. Each sample was placed in two climates at a room temperature of ca. 24 °C (held constant) and two relative humidity (RH) levels: 35% RH (dry climate) and 85% RH (humid climate). These levels were chosen to assess the potential impact of prolonged exposure to very dry or very humid climates. Long-term exposure to such extremes can affect the physicochemical and aesthetic stability of the wood and its treatment, which is crucial to understanding how the archaeological finds will behave in a museum environment. The reference condition was the equilibrium state in the laboratory, i.e., a temperature of ca. 24 °C and approximately 50% relative humidity (this latter uncontrolled).

Due to the limited availability of material, only one sample was used for each climate. However, the two samples were taken from adjacent areas to ensure that their conditions were as similar as possible. These areas were meticulously selected to prevent macroscopically detectable differences in degradation, thereby ensuring greater uniformity in the initial condition of the samples.

The samples were placed in trays inside airtight containers containing saturated salt solutions to maintain a constant relative humidity: magnesium chloride was used for the dry condition and potassium chloride for the humid condition. Temperature and relative humidity were occasionally monitored using devices (Mini TH, XS Instrument, Carpi, Italy) capable of measuring temperature and humidity within the range from −40 to +80 °C and up to 100% RH.

To monitor the samples' behaviour, their mass and dimensions (base area and height) were measured at the start of the experiment. Regular mass measurements were taken until equilibrium was reached. Once equilibrium was reached, the dimensions of the samples were measured again.

Height was measured using a calliper, and the base area was determined using image analysis software on scans taken with a high-resolution scanner (Epson Expression 1640XL, Epson Europe Electronics GmbH, München, Germany) at 800 dpi in TIFF/24-bit RGB format. The images were analysed using ImageJ software version 1.50 (National Institutes of Health, Bethesda, MD, USA). Figure 2 shows an example of how the change in surface area was calculated. To improve accuracy, multiple image analyses were performed on each sample and any outliers or inconsistencies were excluded.

(a) (b)

Figure 2. An example of how the surface area changes were calculated using the ImageJ software: (**a**) the initial area of sample T6 E; (**b**) the same area after conditioning in the climate at 35% RH.

Mass, area and height changes were calculated using the following formulae:

$$\Delta M(\%) = 100 \times \frac{M_{UR} - M_i}{M_i} \quad (1)$$

$$\Delta A(\%) = 100 \times \frac{A_{UR} - A_i}{A_i} \quad (2)$$

$$\Delta H(\%) = 100 \times \frac{A_{UR} - A_i}{A_i} \quad (3)$$

where M, A and H are respectively the mass, area and height of the treated sample after conditioning in the dry or wet climate (*UR* subscript) or before conditioning (*i* subscript).

Each sample was photographed before and after conditioning and any defects or particularities were carefully noted.

3. Results and Discussion

3.1. Identification of Surface Efflorescence

3.1.1. EDS and XRPD Analysis

Figure 3 shows the morphological features of the M12 W ST representative powder sample. It also shows backscattered electron (BSE) imaging highlighting elements with higher atomic numbers, as well as EDS probe results indicating the presence of S, Ca and Fe, in addition to C and O. The results obtained for the other samples are shown in Figures S1–S3, whereas the summary of the various samples is provided in Table 3.

Table 3. List of obtained results through powder microanalysis.

Sample	Na	Si	S	K	Ca	Fe
T6 E	x	x	x	x	x	x
M48 E SE	x	x	x	x	x	x
F14 E PP	x	x	x	x		x
M12 W ST			x		x	x

The data showed that S and Fe were consistently present across all samples, while the presence of the other detected elements (Ca, Si, Na and K) varied depending on the sample considered.

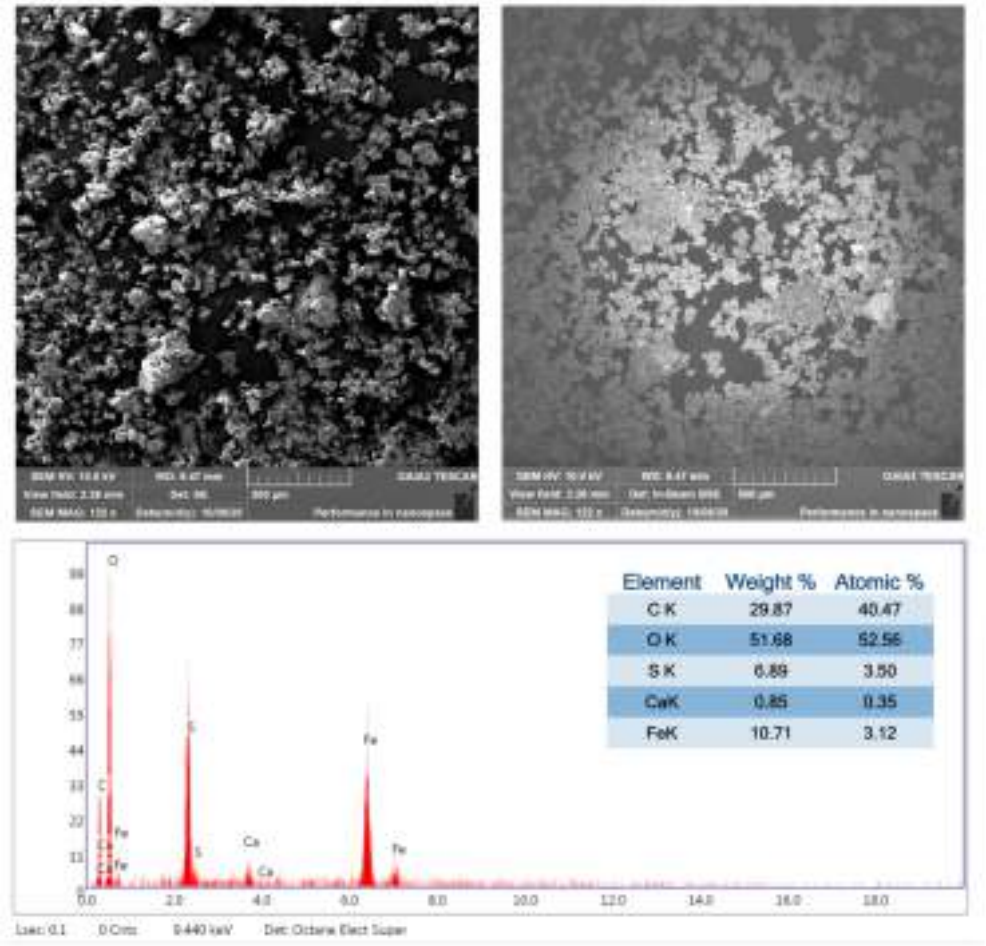

Figure 3. The powders of the sample M12 W ST (stem) on which EDS analyses were conducted. In the top left, morphological images; in the top right, images obtained with backscattered electrons; at the bottom, the powder dispersion spectrum, with the identified elements highlighted.

XRPD analysis (Table 4) was used to attribute these elements to specific mineralogical phases. This analysis showed that all of these phases were mainly constituted by various types of sulphates. In detail, XRPD identified ferrous sulphate tetrahydrate (rozenite) [$FeSO_4 \cdot 4H_2O$]; a hydrated sulphate of Fe, K and Na [$K_2Na_6Fe_7(SO_4)_{12}O_2 \cdot (H_2O)_{18}$]; and gypsum [$CaSO_4 \cdot 2H_2O$]. Iron oxide hydrate ($Fe_2O_3 \cdot H_2O$) was found in samples T6 E, M48 E SE and M12 W ST, while quartz [SiO_2] was found in samples F14 E PP and M12 W ST (Table 4). No Si minerals were found in M48 E SE, probably because they were below the XRPD's detection threshold.

While the presence of quartz can be attributed to the residues of the seabed sediment in which the ship was preserved during burial, the presence of the other inorganic phases is the result of significant degradation caused by prolonged exposure to moisture. The repeated identification of the same compounds, however, suggests a common degradation pattern across the various samples. In fact, it is known that sulphate-reducing bacteria are able to attack wood even in anoxic conditions and produce H_2S during their activity. Therefore, in the presence of iron, iron sulphides can be generated. These compounds accumulate in wood cells and are very stable under reducing (i.e., non-oxidising) conditions. However, when they are exposed to oxygen and humidity, as happens after artefacts are discovered, they form various types of sulphate with the cations present in the environment [25]. Interestingly, the reaction with iron results in the formation of ferrous sulphates rather than ferric sulphates, since in these reactions it is usually only the sulphur that is oxidized and not the iron [25]. The presence of significant amounts of sulphur and iron in the

wood structure often indicates ongoing degradation. For example, amounts of Fe and S were found to range from 30,000 to <600,000 ppm in Chinese shipwrecks showing signs of degradation, and from 4000 to <15,000 ppm in other shipwrecks showing no signs of degradation [26]. Moreover, the presence of ferrous sulphates could theoretically indicate that sulphuric acid has formed in the artefact [27,28], as these can be by-products of iron sulphides reactions producing this acid under oxidising, humid conditions [26]. In any case, the volumetric expansion of ferrous sulphates can damage the structure of decayed wood [29–31]. Even in the absence of sulphates, problems can arise from the presence of ferrous ions, as they can induce the hydrolysis of PEGs and even the oxidation and depolymerisation of cellulose due to the occurrence of the Fenton reaction [32].

Table 4. Summary of the results obtained in X-ray powder diffraction analysis.

Sample	Compounds Identified	Chemical Formula
T6 E	Ferrous sulphate tetrahydrate (Rozenite)	$FeSO_4 \cdot 4H_2O$
	Hydrated sulphate of Fe, K and Na	$K_2Na_6Fe_7(SO_4)_{12}O_2 \cdot (H_2O)_{18}$
	Gypsum	$CaSO_4 \cdot 2H_2O$
	Iron oxide hydrate	$Fe_2O_3 \cdot H_2O$
M48 E SE	Ferrous sulphate tetrahydrate (Rozenite)	$FeSO_4 \cdot 4H_2O$
	Hydrated sulphate of Fe, K and Na	$K_2Na_6Fe_7(SO_4)_{12}O_2 \cdot (H_2O)_{18}$
	Gypsum	$CaSO_4 \cdot 2H_2O$
	Iron oxide hydrate	$Fe_2O_3 \cdot H_2O$
F14 E PP	Ferrous sulphate tetrahydrate (Rozenite)	$FeSO_4 \cdot 4H_2O$
	Hydrated sulphate of Fe, K and Na	$K_2Na_6Fe_7(SO_4)_{12}O_2 \cdot (H_2O)_{18}$
	Gypsum	$CaSO_4 \cdot 2H_2O$
	Quartz	SiO_2
M12 W ST	Ferrous sulphate tetrahydrate (Rozenite)	$FeSO_4 \cdot 4H_2O$
	Hydrated sulphate of Fe, K and Na	$K_2Na_6Fe_7(SO_4)_{12}O_2 \cdot (H_2O)_{18}$
	Gypsum	$CaSO_4 \cdot 2H_2O$
	Quartz	SiO_2
	Iron oxide hydrate	$Fe_2O_3 \cdot H_2O$

3.1.2. ATR-FTIR Analysis

The FTIR spectra collected from the efflorescence were similar in shape (Figure 4), with the differences mainly being related to varying levels of PEG 4000 contamination.

Figure 5 shows the presence of PEG signals in the analysed powders for the representative sample F14 E PP, compared with the spectrum acquired from a solidified whitish drop found on the surface of one of the ship's elements. It was determined that this whitish drop was constituted by PEG by comparing the spectrum of the drop with that of PEG 4000 available in the laboratory; the two spectra overlapped perfectly (Figure S4). In this case, the bands specifically attributable to PEG are primarily those related to the vibrations of the CH_2 group: the stretching mode at 2880 cm^{-1}, the scissoring mode at 1466 cm^{-1}, the wagging mode at 1340 cm^{-1}, the twisting mode at 1280 cm^{-1} and 1240 cm^{-1} (the latter of which is associated with C–C stretching), and the rocking mode at 960 cm^{-1} and 840 cm^{-1} [33]. However, these signals were not present in the same amounts in all the samples analysed (F14 E PP and T6 E had more of these bands than M48 E SE and M12 W ST). In contrast, the vibrations at 1060 and 1098 cm^{-1}, which are usually very intense in PEG and are associated with CH_2 + C–O stretching, were not observable in our case because they are covered by other signals attributable to the inorganic phases present.

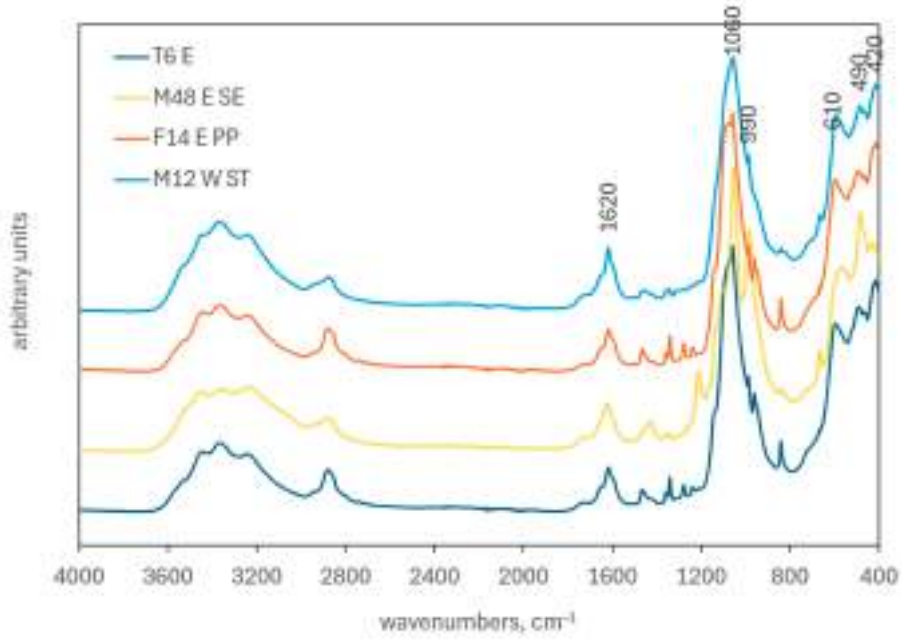

Figure 4. Comparison of ATR-FTIR spectra obtained from the powders collected from the surface efflorescence of the ship: T6 E (dark blue curve), M48 E SE (orange curve), F14 E PP (red curve), and M12 W ST (light blue curve). The spectra were Vector-normalized over the entire acquisition range.

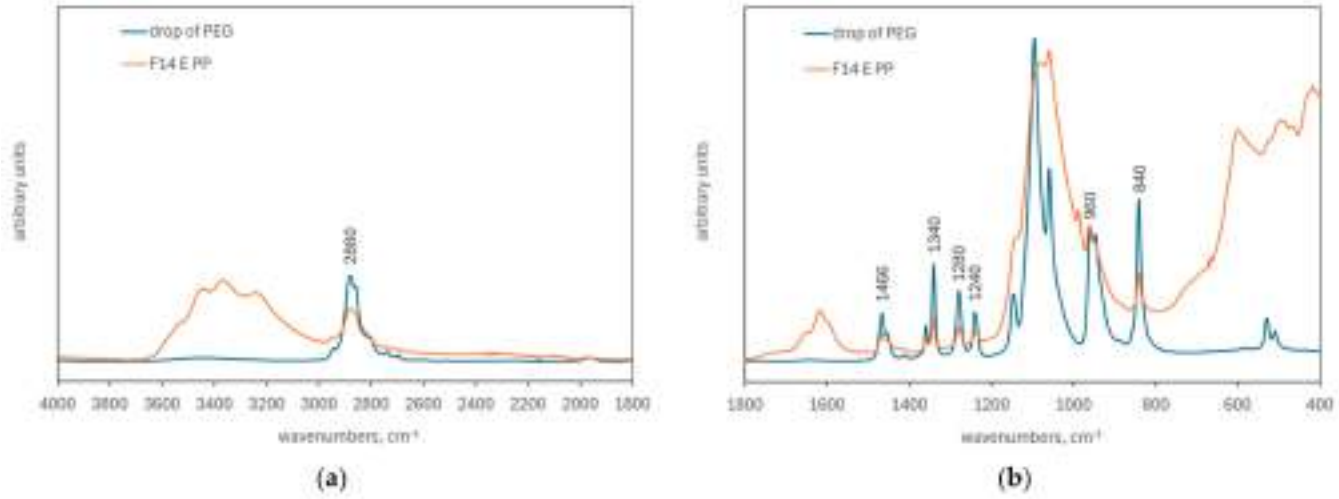

Figure 5. Comparison between the spectra of the F14 E PP sample (red curve) and a drop of PEG (dark blue curve). For better readability, spectra are divided between 1800–4000 cm^{-1} (**a**) and 400–1800 cm^{-1} (**b**). The spectra were Vector normalized in the range of 1800–700 cm^{-1}.

In fact, the ATR-FTIR analysis confirmed the presence of sulphate-containing minerals in all four samples, in addition to PEG. Sulphate ions in solutions can be identified by two bands: one broad peak at around 1100 cm^{-1} due to the antisymmetric stretching of the SO_4^{2-} ion and one at around 610 cm^{-1} [25,34]. These two IR-active vibration modes are known as υ_3 and υ_4, respectively. In addition, the various coordination possibilities in inorganic hydrated salts induce a change in crystal symmetry, causing other bands to become IR-active. These bands include those at around 975 cm^{-1} and 450 cm^{-1}, known as υ_1 and υ_2, respectively [25,35]. However, shifts or splits in signals are usually observed in mineral phases, particularly when other ions (such as Na and K) are included in the crystal structure due to changes in bond length and sulphate molecule symmetry [36]. In all samples, the most intense band is located at 1060 cm^{-1} (1050 cm^{-1} for M48 E SE), while the other bands specifically attributable to sulphate-containing minerals are located

at 610 cm^{-1} (though absent in M48 E SE) and 990 cm^{-1}. Thus, a shift of 50–60 cm^{-1} was observed for the v_3 vibration mode and 15 cm^{-1} for the v_1 vibration mode. This is not unusual in minerals with a complex structure [34].

In our case, the attributions are complicated by the fact that at least one of the mineral phases identified by XRPD analysis, namely rozenite ($FeSO_4 \cdot 4H_2O$), can spontaneously change its hydration state depending on the relative humidity and temperature of the environment: different phases can form as a function of temperature and humidity conditions, ranging from the heptahydrate ($FeSO_4 \cdot 7H_2O$) to the monohydrate ($FeSO_4 \cdot H_2O$) structures [35]. For example, it has previously been reported that the three hydrated forms of ferrous sulphate followed seasonal patterns in the efflorescence found on the Newark's Museum collections: melanterite (heptahydrate) was more prevalent in humid summers (>60% RH), while in drier winters (<40% RH), it dehydrated into rozenite (tetrahydrate) and szomolnokite (monohydrate) [25].

Furthermore, in our case, the vibration modes of the sulphate group are expected to lie in the lower wavenumber region (400–650 cm^{-1}), where they overlap with the Fe–O stretching mode of iron oxides. This makes the interpretation of FTIR spectra even more difficult. These vibrations include signals at 490 cm^{-1} and 420 cm^{-1}.

The presence of the signal at 1620 cm^{-1}, due to the OH bending mode, and the signals in the region of 2800–3800 cm^{-1}, due to the overlapping OH stretching vibration of the hydrated phases in different structures, confirms the hydration of the present mineral phases, including iron oxides.

In general, quartz was difficult to identify in the samples, as found in the XRPD analysis, because the Si–O bond shows strong absorption in the 1060–1080 cm^{-1} range, which overlaps with the most intense sulphate band, and at around 460 cm^{-1}, which overlaps with the iron oxide bands. Only the third quartz characteristic band at around 780 cm^{-1} (Si–O symmetric stretching [37]) was detected as a small band close to the PEG band at 840 cm^{-1}, and this was only observed in sample M12 W ST. This suggests that, where detectable, quartz was present in very small amounts.

It is worth noting that the spectrum of M48 E SE sample was slightly different from the others. This sample showed signals, namely the bands at 1212 and 1428 cm^{-1}, that were either absent or less prominent in the other samples. These vibrations have not been assigned, but they could be associated with organic salts (e.g., oxalates) or carbonates (the latter possibility would be further confirmed by the presence of the bands at 1420, 872 and 670 cm^{-1}). The absence of these compounds from the XRPD analysis implies that they were not well crystallized. These results are consistent with those of previous studies in which similar compounds were found in waterlogged archaeological wood, confirming the presence of gypsum, hydrated iron (II) sulphate, and potentially organic compounds [38].

3.2. Conditioning Tests

Tables 5 and 6 summarise the results of the measurements of the mass, surface area and height of the samples at the end of the conditioning period in the two different climates. These tables also present the percentage variation in these parameters.

In the 35% RH climate, the samples stabilised after 35–40 days of conditioning (Figure S5). The data indicate that no substantial differences in behaviour were observed between the dry climate and the initial conditions, in terms of both mass and dimensions. Specifically, the samples exhibited an average mass loss of less than 1% (−0.89%, with a standard deviation of 0.12%), a 0.4% reduction in surface area (stand. dev. 1.0%), and minimal changes in height. The high dimensional stability observed in the dry climate is due to the presence of PEG 4000, which is known for its slow moisture loss due to its composition and partial crystallinity [39–41]. In several cases, slight variations in behaviour among the

different samples can be attributed to this factor. For example, sample 23 exhibited the greatest mass loss (−1.23%). This sample had a PEG weight percentage of 72%, which is lower than the average PEG content of 83%. The PEG content values were estimated from extraction tests performed on a subset of the ship's wood samples, following cold-water extraction procedure, and detailed results of this analysis are described and discussed in [20].

Table 5. Mass, surface area and height changes for the various samples conditioned in the dry climate (35% RH). Initial and final values are also given.

Sample ID	M_i, g	A_i, mm^2	H_i, mm	M_{35}, g	A_{35}, mm^2	H_{35}, mm	ΔM, %	ΔA, %	ΔH, %
6	0.51	61.0	7.91	0.51	61.2	7.86	−0.98	0.4	−0.63
8	1.22	139.5	7.51	1.21	141.4	7.51	−0.76	1.4	0.00
9	1.23	166.9	7.71	1.21	164.8	7.52	−1.03	−1.3	−2.46
11	0.38	40.9	7.88	0.38	40.5	7.87	−0.81	−1.1	−0.13
12	1.02	101.9	7.91	1.00	100.2	7.88	−1.01	−1.7	−0.38
13	0.50	68.9	6.45	0.50	69.2	6.62	−0.88	0.5	2.64
14	3.23	266.3	10.25	3.21	267.5	10.21	−0.73	0.5	−0.39
15	5.93	667.8	7.7	5.88	669.0	7.72	−0.90	0.2	0.26
16	1.49	199.3	6.58	1.48	199.6	6.59	−0.93	0.1	0.15
17	0.86	124.3	6.18	0.85	123.3	6.18	−0.83	−0.8	0.00
18	3.07	348.1	7.2	3.04	341.1	7.26	−0.92	−2.0	0.83
20	2.73	326.0	7.71	2.71	324.8	7.84	−0.80	−0.3	1.69
21	1.24	160.4	7.36	1.23	159.8	7.33	−0.93	−0.4	−0.41
22	1.39	148.3	7.32	1.38	146.4	7.31	−0.85	−1.3	−0.14
23	1.09	183.6	7.63	1.08	184.5	7.62	−1.23	0.5	−0.13
24	0.75	84.0	7.33	0.74	83.6	7.33	−0.74	−0.5	0.00
25	1.64	179.8	7.71	1.62	176.9	7.71	−0.82	−1.7	0.00
						average	−0.89	−0.4	0.05
						std. dev.	0.12	1.0	1.05

Table 6. Mass, surface area and height changes for the various samples conditioned in the humid climate (85% RH). Initial values and final values are also given.

Sample ID	M_i, g	A_i, mm^2	H_i, mm	M_{85}, g	A_{85}, mm^2	H_{85}, mm	ΔM, %	ΔA, %	ΔH
6	0.40	43.0	7.83	0.44	broken	7.90	11.80	–	0.89
8	1.12	129.9	7.48	1.22	131.4	7.41	9.56	1.1	−0.94
9	1.19	154.4	6.96	1.32	165.2	6.96	11.09	7.0	0.00
11	0.42	45.2	7.85	0.46	47.2	7.85	10.18	4.4	0.00
12	1.05	111.5	7.91	1.18	broken	7.89	12.29	–	−0.25
13	0.51	65.7	6.59	0.56	71.1	6.66	11.42	8.2	1.06
14	3.02	258.9	10.09	3.35	265.5	10.09	10.70	2.6	0.00
15	5.26	671.8	7.8	5.93	712.7	7.86	12.71	6.1	0.77
16	1.52	182.4	6.53	1.71	broken	6.53	12.13	–	0.00
17	0.72	104.4	6.56	0.79	109.4	6.72	10.71	4.7	2.44
18	2.02	236.5	7.3	2.24	broken	7.27	11.20	–	−0.41
20	2.99	306.4	7.87	3.31	318.3	7.88	10.69	3.9	0.13
21	1.59	177.8	7.35	1.77	broken	7.34	11.21	–	−0.14
22	1.16	144.0	7.48	1.30	153.5	7.42	11.50	6.6	−0.80
23	0.97	187.4	7.78	1.09	194.2	7.78	11.74	3.6	0.00
24	0.71	79.9	7.33	0.79	83.1	7.28	11.47	4.0	−0.68
25	1.37	169.8	7.63	1.52	179.6	7.48	10.66	5.8	−1.97
						average	11.24	4.8	0.01
						std. dev.	0.79	2.0	0.95

Despite moisture loss, some samples exhibited an apparent increase in surface area between 0.5% and 1.4%. This phenomenon, observed in samples 8, 13, 14 and 23, was investigated using an alternative image analysis approach involving the comparison of the areas through overlapping layers (Figure S6). This approach confirmed the surface area increase and revealed that it was primarily due to minor distortions rather than actual material swelling.

Samples conditioned at 85% RH exhibited markedly different behaviour compared to those conditioned at 35% RH. Stabilisation was only achieved after 425 days, during which time an increase in the internal humidity of the material was observed (Figure S7). This ultimately resulted in the visible migration of PEG in some samples. Humidity adsorption resulted in an average mass increase of 11.2% (stand. dev. 0.8%) and an average surface area increase of 4.8% (stand. dev. 0.2%). However, these increases in surface area due to swelling were associated with the appearance of fractures and distortions. In some cases the samples fractured, as was observed in samples 6, 12, 16, 18 and 21. This behaviour is likely to be associated with that of the PEG, which can undergo a phase transition due to dissolution in condensed humidity under prolonged high humidity conditions. The PEG can then migrate to the surface, thereby altering the sample's structure. PEG migration and leaching from the wood surface has been observed in other cases, altering the material's appearance and complicating future interventions [42]. Interestingly, in our case, PEG migration was not connected with a noticeable change in mass, probably because the consolidant mass was redistributed inside the sample before a significant increase or decrease in mass occurred due to moisture adsorption or PEG leaching, respectively, when the process was stopped.

4. Conclusions

The findings suggest that the elements of the *Iulia Felix* shipwreck have undergone natural degradation processes, influenced by environmental factors and previous conservation treatments. The presence of hydrated ferrous sulphates on all analysed surfaces suggests corrosion processes typically associated with metal components. This corrosion originates in marine environments and progresses in humid, oxidative conditions following recovery. The presence of gypsum, which is common in underwater environments, may also contribute to degradation by generating internal stresses that weaken the material.

These chemical transformations represent potential degradation pathways, which are particularly significant given the wood's poor state of preservation. However, the absence of comparable analyses at the time of discovery implies it is not possible to determine whether degradation has progressed over the past 20 years.

The presence of hydrated ferrous sulphates highlights the need for ongoing monitoring due to their impact on structural integrity. Additionally, the presence of PEG in the efflorescence indicates that environmental conditions after treatment promoted its gradual migration to the surface, likely accelerated by humidity. This migration may have led to the formation of surface crusts, indicating a loss of consolidant from the interior, which could affect long-term physicochemical and aesthetic stability.

Environmental testing confirmed that prolonged exposure to high humidity (85% RH) has a significantly greater impact than exposure to drier conditions (35% RH). Under humid conditions, samples exhibited dimensional expansion, PEG exudation and, in some cases, fracturing. This demonstrates that PEG-treated wood becomes destabilised in environments with high humidity. Despite being considered stable in the short term and only mildly hygroscopic, PEG 4000 did not prevent degradation and may have contributed to structural decay, particularly under fluctuating moisture conditions during storage.

These findings emphasise the importance of environmental control in conservation strategies. To prevent swelling, microfractures, and PEG migration, it is essential to main-

tain stable relative humidity within a moderately dry range of approximately 50%–60%. These requirements have been incorporated into the design of the new museum environment and the planned upgrade to the climate control systems.

Furthermore, the study highlights the need for ongoing monitoring of artefacts that have previously been treated, and the necessity of developing more effective conservation strategies, particularly for treatments involving PEG. This includes exploring more stable alternatives to reduce the risk of degradation.

Supplementary Materials: The following supporting information can be downloaded at: https://www.mdpi.com/article/10.3390/f17050627/s1, Figure S1: The powders of the sample M48 E SE (semi-ordered) on which EDS analyses were conducted. In the top left, morphological images; in the top right, images obtained with backscattered electrons; at the bottom, the powder dispersion spectrum, with the identified elements highlighted; Figure S2: The powders of the sample F14 E PP on which EDS analyses were conducted. In the top left, morphological images; in the top right, images obtained with backscattered electrons; at the bottom, the powder dispersion spectrum, with the identified elements highlighted; Figure S3: The powders of the sample T6 E on which EDS analyses were conducted. In the top left, morphological images; in the top right, images obtained with backscattered electrons; at the bottom, the powder dispersion spectrum, with the identified elements highlighted; Figure S4: Comparison between the spectra of the whitish drop found on the surface of one of the ship's elements (blue curve) with that of PEG 4000 available in the laboratory (orange curve). The two spectra overlapped perfectly and were shifted vertically for better readability; Figure S5: Average relative mass variation of the samples over time during the conditioning period in a dry climate at 35% relative humidity (RH). The upper and lower curves represent the 95% confidence interval extremes of the data; Figure S6: Some examples of the processing that took place after the initial area level was super-imposed (in red) on samples that had shown an increase in area following a decrease in ambient humidity, before and after conditioning at 35%. The arrows indicate the areas where the surface area has increased; Figure S7: Average relative mass variation of the samples over time during the conditioning period in a humid climate at 85% relative humidity (RH). The upper and lower curves represent the 95% confidence interval extremes of the data.

Author Contributions: Conceptualization, B.P. and N.M.; Methodology, B.P. and E.P.; Validation, E.P., B.P. and E.C.; Investigation, E.P. and S.L.; Resources, G.M. and M.N.; Writing—Original Draft Preparation, E.P., B.P. and N.M.; Writing—Review & Editing, E.P., N.M., G.M., E.C., M.N. and B.P.; Visualization, B.P. and E.P.; Supervision, B.P.; Project Administration, G.M. and M.N.; Funding Acquisition, M.N. All authors have read and agreed to the published version of the manuscript.

Funding: This research was funded by the Polo Museale of Friuli Venezia Giulia, currently Museo storico e Parco del Castello di Miramare-Direzione regionale Musei nazionali Friuli Venezia Giulia (Italian Ministry of Culture).

Data Availability Statement: Dataset available on request from the authors.

Acknowledgments: The diagnostic analyses were funded by the Polo Museale of Friuli Venezia Giulia, currently Museo storico e Parco del Castello di Miramare-Direzione regionale Musei nazionali Friuli Venezia Giulia (Italian Ministry of Culture), with the ultimate goal of providing a scientific basis for designing the exhibition spaces and display supports on which the ship was reconstructed. The authors would like to thank Elena Braidotti and Charlotte Montanaro for helping to revise part of the text.

Conflicts of Interest: Representatives of the funding institution were involved in writing the manuscript. The authors declare no conflicts of interest.

References

1. Dell'Amico, P. Il Relitto Di Grado: Considerazioni Preliminari. *Archeol. Subacquea Studi Ric. E Doc.* **1997**, *2*, 93–128.
2. Beltrame, C.; Gaddi, D. Documentazione e Analisi Degli Elementi Strutturali Dello Scafo Della Nave Romana Di Grado (GO). *Archeololgia Delle Acque* **2000**, *4*, 99–102.
3. Beltrame, C.; Gaddi, D. Preliminary Analysis of the Hull of the Roman Ship from Grado, Gorizia, Italy. *Int. J. Naut. Archaeol.* **2007**, *36*, 138–147. [CrossRef]
4. Giacobelli, M. I Vetri Del Relitto Di Grado. In *Atti del Convegno Nazionale di Archeologia Subacquea (Anzio)*; Edipuglia: Bari, Italy, 1996; pp. 311–314.
5. Auriemma, R. Le Anfore Del Relitto Di Grado e Il Loro Contenuto. *MEFRA Mélanges L'école Française Rome. Antiq.* **2000**, *112*, 27–51. [CrossRef]
6. Costa, E.; Beltrame, C. 3D Modelling from Archive and Legacy Data: Preliminary Data Processing on the Roman Shipwreck Grado I. *Archeol. Calc.* **2021**, *32*, 156–166. [CrossRef]
7. Contessa, A.; Novello, M.; Condò, F. Il Nuovo Museo Di Archeologia Subacquea Dell'Alto Adriatico Di Grado (GO). In *Proceedings of the Allestire l'archeologia. Progetti in Corso e Nuove Proposte per i Musei e i Parchi Archeologici Nazionali, Atti del Convegno a Cura di*; Osanna, M., Bressan, M., Eds.; Franco Cosimo Panini: Modena, Italy, 2024; pp. 207–215.
8. Fors, Y. Sulfur-Related Conservation Concerns in Marine Archaeological Wood: The Origin, Speciation and Distribution of Accumulated Sulfur with Some Remedies for the Vasa. Doctoral Dissertation, Stockholm University, Stockholm, Sweden, 2008.
9. Fors, Y.; Jalilehvand, F.; Damian Risberg, E.; Björdal, C.; Phillips, E.; Sandström, M. Sulfur and Iron Analyses of Marine Archaeological Wood in Shipwrecks from the Baltic Sea and Scandinavian Waters. *J. Archaeol. Sci.* **2012**, *39*, 2521–2532. [CrossRef]
10. Almkvist, G.; Hocker, E.; Sahlstedt, M. *Iron Removal from Waterlogged Wood*; Swedish University of Agricultural Sciences, SLU Repro: Uppsala, Sweden, 2013.
11. Kılıç, A.G.; Kılıç, N.; Arnold, D.C. Analyses of Sulfur and Iron in Waterlogged Archaeological Wood: The Case of Polyethylene-Glycol-Treated Yenikapı 12 Shipwreck. *Forests* **2023**, *14*, 530. [CrossRef]
12. Mortensen, M.N.; Egsgaard, H.; Hvilsted, S.; Shashoua, Y.; Glastrup, J. Characterisation of the Polyethylene Glycol Impregnation of the Swedish Warship Vasa and One of the Danish Skuldelev Viking Ships. *J. Archaeol. Sci.* **2007**, *34*, 1211–1218. [CrossRef]
13. Pearson, C. *Conservation of Marine Archaeological Objects*; Butterworth-Heinemann (An Imprint of Elsevier): Oxford, UK, 2014; ISBN 978-1-4832-9465-0.
14. Hoffmann, P. To Be and to Continue Being a Cog: The Conservation of the Bremen Cog of 1380. *Int. J. Naut. Archaeol.* **2001**, *30*, 129–140. [CrossRef]
15. Glastrup, J.; Shashoua, Y.; Egsgaard, H.; Nordvig Mortensen, M. Formic and Acetic Acids in Archaeological Wood. A Comparison between the Vasa Warship, the Bremen Cog, the Oberländer Boat and the Danish Viking Ships. *Holzforschung* **2006**, *60*, 259–264. [CrossRef]
16. Dedic, D.; Iversen, T.; Ek, M. Cellulose Degradation in the Vasa: The Role of Acids and Rust. *Stud. Conserv.* **2013**, *58*, 308–313. [CrossRef]
17. Baird, J.A.; Olayo-Valles, R.; Rinaldi, C.; Taylor, L.S. Effect of Molecular Weight, Temperature, and Additives on the Moisture Sorption Properties of Polyethylene Glycol. *J. Pharm. Sci.* **2010**, *99*, 154–168. [CrossRef]
18. Majka, J.; Zborowska, M.; Fejfer, M.; Waliszewska, B.; Olek, W. Dimensional Stability and Hygroscopic Properties of PEG Treated Irregularly Degraded Waterlogged Scots Pine Wood. *J. Cult. Herit.* **2018**, *31*, 133–140. [CrossRef]
19. Pecoraro, E.; Pizzo, B.; Salvini, A.; Macchioni, N. Dynamic Mechanical Analysis (DMA) at Room Temperature of Archaeological Wood Treated with Various Consolidants. *Holzforschung* **2019**, *73*, 757–772. [CrossRef]
20. Pizzo, B.; Li, R.; Macchioni, N.; Sozzi, L.; Yin, Y.; Musina, G.; Novello, M.; Pecoraro, E. Diagnostic Characterisation of Wood from Archaeological Artefacts Already Treated with Polyethylene Glycols. 2026; *manuscript in preparation*.
21. Remazeilles, C.; Leveque, F.; Minjacq, M.; Refait, P.; Sanchez, C.; Jézégou, M.-P. Characterisation of Iron (II) Sulfides in Wet Archaeological Woods: The Wreck of Mandirac (IV Th Century, Antique Ports of Narbonne, France). In Proceedings of the 13th ICOM-CC Group on Wet Organic Archaeological Materials Conference (WOAM 2016), Florence, Italy, 16–20 May 2016.
22. Rémazeilles, C.; Saheb, M.; Neff, D.; Guilminot, E.; Tran, K.; Bourdoiseau, J.-A.; Sabot, R.; Jeannin, M.; Matthiesen, H.; Dillmann, P.; et al. Microbiologically Influenced Corrosion of Archaeological Artefacts: Characterisation of Iron(II) Sulfides by Raman Spectroscopy. *J. Raman Spectrosc.* **2010**, *41*, 1425–1433. [CrossRef]
23. KILIÇ, A.G.; Kilic, N.; Akgün, C. The Importance of Using Multiple Analyses Techniques to Determine the Physical Condition of the Waterlogged Wood Near the Corroded Parts. *Wood Res.* **2021**, *66*, 1046–1054. [CrossRef]
24. Fors, Y.; Jalilehvand, F.; Sandström, M. Analytical Aspects of Waterlogged Wood in Historical Shipwrecks. *Anal. Sci.* **2011**, *27*, 785–792. [CrossRef] [PubMed]
25. Rouchon, V.; Badet, H.; Belhadj, O.; Bonnerot, O.; Lavédrine, B.; Michard, J.; Miska, S. Raman and FTIR Spectroscopy Applied to the Conservation Report of Paleontological Collections: Identification of Raman and FTIR Signatures of Several Iron Sulfate Species Such as Ferrinatrite and Sideronatrite. *J. Raman Spectrosc.* **2012**, *43*, 1265–1274. [CrossRef]

26. Song, K.; Yin, Y.; Salmén, L.; Xiao, F.; Jiang, X. Changes in the Properties of Wood Cell Walls during the Transformation from Sapwood to Heartwood. *J. Mater. Sci.* **2014**, *49*, 1734–1742. [CrossRef]
27. Almkvist, G.; Persson, I. Extraction of Iron Compounds from Wood from the Vasa. *Holzforschung* **2006**, *60*, 678–684. [CrossRef]
28. Fors, Y.; Sandström, M. Sulfur and Iron in Shipwrecks Cause Conservation Concerns. *Chem. Soc. Rev.* **2006**, *35*, 399–415. [CrossRef]
29. Pelé-Meziani, C.; Macchioni, N.; Sozzi, L.; Guilminot, E.; Lemoine, G.; Pizzo, B.; Mevellec, J.Y.; Pecoraro, E.; Monachon, M. Assessment of Various Iron Extraction Treatments on Waterlogged Archaeological Oak. *Forests* **2023**, *14*, 1834. [CrossRef]
30. Sandström, M.; Jalilehvand, F.; Persson, I.; Gelius, U.; Frank, P.; Hall-Roth, I. Deterioration of the Seventeenth-Century Warship Vasa by Internal Formation of Sulphuric Acid. *Nature* **2002**, *415*, 893–897. [CrossRef]
31. Pecoraro, E.; Pelé-Meziani, C.; Macchioni, N.; Lemoine, G.; Guilminot, E.; Shen, D.; Pizzo, B. The Removal of Iron from Waterlogged Archaeological Wood: Efficacy and Effects on the Room Temperature Wood Properties. *Wood Mater. Sci. Eng.* **2023**, *18*, 672–689. [CrossRef]
32. Monachon, M.; Albelda-Berenguer, M.; Pelé, C.; Cornet, E.; Guilminot, E.; Rémazeilles, C.; Joseph, E. Characterization of Model Samples Simulating Degradation Processes Induced by Iron and Sulfur Species on Waterlogged Wood. *Microchem. J.* **2020**, *155*, 104756. [CrossRef]
33. Brogly, M.; Bistac, S.; Bindel, D. Adsorption and Structuration of PEG Thin Films: Influence of the Substrate Chemistry. *Polymers* **2024**, *16*, 1244. [CrossRef]
34. Peak, D.; Ford, R.G.; Sparks, D.L. An in Situ ATR-FTIR Investigation of Sulfate Bonding Mechanisms on Goethite. *J. Colloid Interface Sci.* **1999**, *218*, 289–299. [CrossRef]
35. Lacalamita, M.; Ventruti, G.; Della Ventura, G.; Radica, F.; Mauro, D.; Schingaro, E. In Situ High-Temperature X-Ray Powder Diffraction and Infrared Spectroscopic Study of Melanterite, $FeSO_4 \cdot 7H_2O$. *Minerals* **2021**, *11*, 392. [CrossRef]
36. Myneni, S.C.B. X-Ray and Vibrational Spectroscopy of Sulfate in Earth Materials. *Rev. Mineral. Geochem.* **2000**, *40*, 113–172. [CrossRef]
37. Saikia, J.B. Spectroscopic Estimation of Geometrical Structure Elucidation in Natural SiO_2 Crystal. *J. Mater. Phys. Chem.* **2014**, *2*, 28–33. [CrossRef]
38. Rémazeilles, C.; Tran, K.; Guilminot, E.; Conforto, E.; Refait, P. Study of Fe(II) Sulphides in Waterlogged Archaeological Wood. *Stud. Conserv.* **2013**, *58*, 297–307. [CrossRef]
39. Grattan, D.W. A Practical Comparative Study of Several Treatments for Waterlogged Wood. *Stud. Conserv.* **1982**, *27*, 124. [CrossRef]
40. Christensen, M.; Kutzke, H.; Hansen, F.K. New Materials Used for the Consolidation of Archaeological Wood–Past Attempts, Present Struggles, and Future Requirements. *J. Cult. Herit.* **2012**, *13*, S183–S190. [CrossRef]
41. Li, R.; Wu, Y.; Bai, Z.; Guo, J.; Chen, X. Effect of Molecular Weight of Polyethylene Glycol on Crystallization Behaviors, Thermal Properties and Tensile Performance of Polylactic Acid Stereocomplexes. *RSC Adv.* **2020**, *10*, 42120–42127. [CrossRef]
42. Jo, A.H.; Lee, K.-H.; Choi, T.-H.; Go, I.H.; Seo, J.-W. Changes in the Amount of PEG Free-Flowing Back from PEG-Treated Waterlogged Archaeological Wood and the Compressive Strength According to Relative Humidity Conditions. *J. Conserv. Sci.* **2020**, *36*, 225–235. [CrossRef]

Disclaimer/Publisher's Note: The statements, opinions and data contained in all publications are solely those of the individual author(s) and contributor(s) and not of MDPI and/or the editor(s). MDPI and/or the editor(s) disclaim responsibility for any injury to people or property resulting from any ideas, methods, instructions or products referred to in the content.